



OPEN ACCESS

EDITED BY

Anna Hankin,
Imperial College London,
United Kingdom

REVIEWED BY

Juqin Zeng,
Italian Institute of Technology (IIT), Italy
Isaac Holmes-Gentle,
Swiss Federal Institute of Technology
Lausanne, Switzerland

*CORRESPONDENCE

Johan A. Martens,
johan.martens@kuleuven.be

SPECIALTY SECTION

This article was submitted to
Electrochemical Engineering,
a section of the journal
Frontiers in Chemical Engineering

RECEIVED 26 August 2022

ACCEPTED 24 October 2022

PUBLISHED 09 November 2022

CITATION

Thijs B, Hanssens L, Heremans G,
Wangermez W, Rongé J and Martens JA
(2022), Demonstration of a three
compartment solar electrolyser with gas
phase cathode producing formic acid
from CO₂ and water using Earth
abundant metals.
Front. Chem. Eng. 4:1028811.
doi: 10.3389/fceng.2022.1028811

COPYRIGHT

© 2022 Thijs, Hanssens, Heremans,
Wangermez, Rongé and Martens. This is
an open-access article distributed
under the terms of the [Creative
Commons Attribution License \(CC BY\)](#).
The use, distribution or reproduction in
other forums is permitted, provided the
original author(s) and the copyright
owner(s) are credited and that the
original publication in this journal is
cited, in accordance with accepted
academic practice. No use, distribution
or reproduction is permitted which does
not comply with these terms.

Demonstration of a three compartment solar electrolyser with gas phase cathode producing formic acid from CO₂ and water using Earth abundant metals

Barbara Thijs, Lucas Hanssens, Gino Heremans,
Wauter Wangermez, Jan Rongé and Johan A. Martens*

Centre for Surface Chemistry and Catalysis: Characterization and Application Team (COK-KAT),
Department of Microbial and Molecular Systems, KU Leuven, Leuven, Belgium

A three compartment solar formic acid generator was built using a Sn on Cu foam cathode and NiFe anode. A bipolar combination of a Fumasep FAD-PET-75 and Nafion 117 membrane was mounted between anode and middle compartment, which was filled with Amberlyst 15H ion exchanger beads. A Fumasep FAD-PET-75 membrane separated the middle compartment from the cathode. The generator was powered with a photovoltaic panel and fed with gaseous CO₂ and water. Diluted formic acid solution was produced by flowing water through the middle compartment. Common PV-EC devices are operated using aqueous electrolyte and produce aqueous formate. In our PV-EC device, formic acid is produced straight away, avoiding the need for downstream operations to convert formate to formic acid. The electrolyser was matched with solar photovoltaic cells achieving a coupling efficiency as high as 95%. Our device produces formic acid at a faradaic efficiency of ca. 31% and solar-to-formic acid efficiency of ca. 2%. By producing formic acid from CO₂ and water without any need of additional chemicals this electrolyser concept is attractive for use at remote locations with abundant solar energy. Formic acid serves as a liquid renewable fuel or chemical building block.

KEYWORDS

CCU, formic acid, renewable fuel, three compartment electrolyser, solar efficiency

1 Introduction

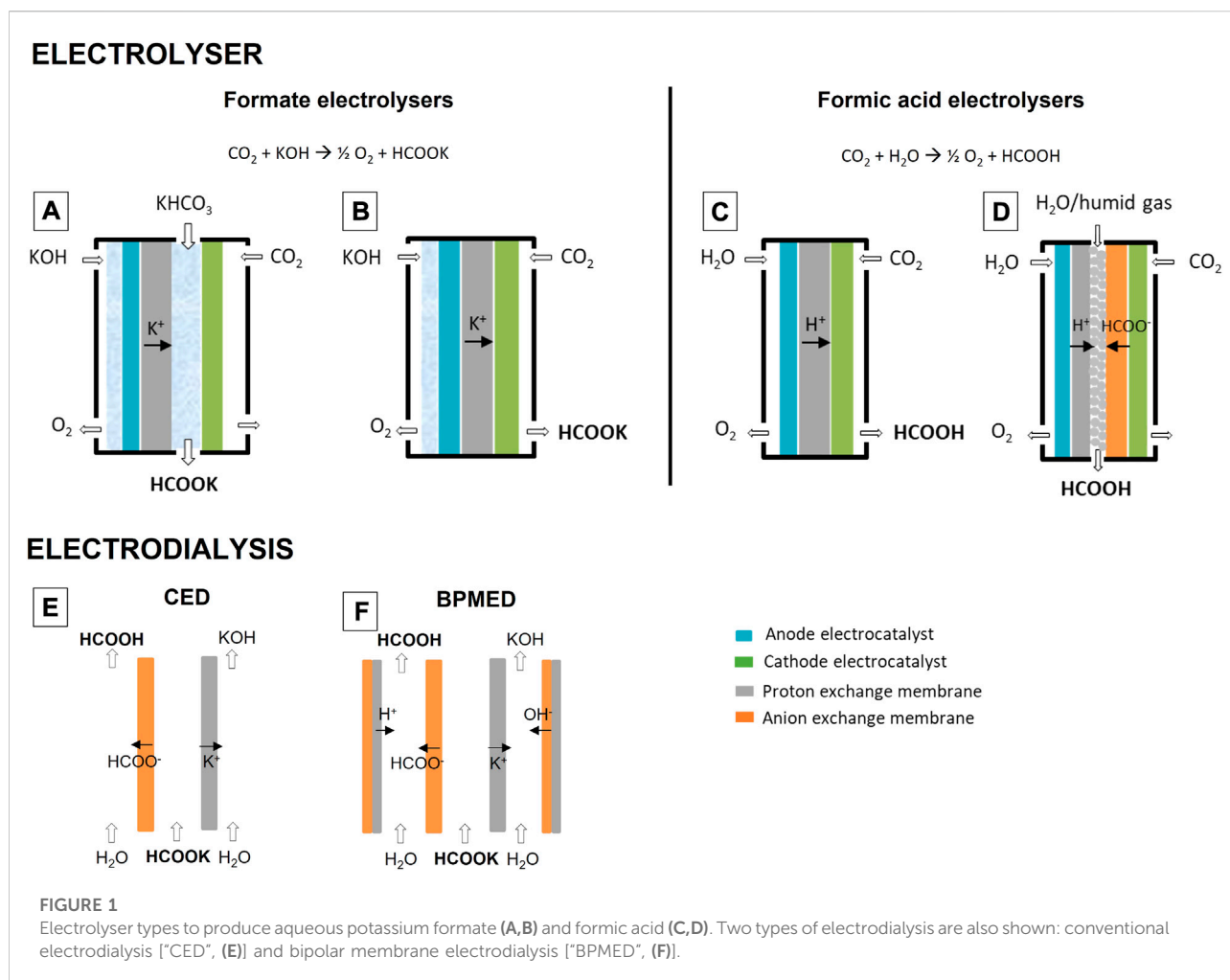
Formic acid is a carboxylic acid with a global market of ca. 750,000 tonnes in 2020, growing annually by ca. 4.5%. ([Global Formic Acid Market Report, 2022](#)) Besides its traditional large-scale industrial production from CO from fossil carbon, new synthesis pathways are being developed to produce it from CO₂ in the context of carbon capture

and utilization (CCU). One of these pathways is electrolysis in which formic acid is produced from CO₂ and H₂O (CO₂ + H₂O → ½ O₂ + HCOOH).

Electrolysis requires electrical power, which can be provided by the grid or directly from a renewable power source such as solar photovoltaics or wind turbines. The technological targets of electrolyser design are dependent on the situation. Grid-connection can ensure continuous operation. The technological targets of electrolyser design for this application are obtaining high current densities, high CO₂ and electric power utilization efficiencies and long-term stability. Gas diffusion electrode (GDE)-type electrodes, (Higgins et al., 2019; Song et al., 2019), gas-trapping strategies, (García de Arquer et al., 2020; Khan et al., 2021a; Yue et al., 2021), nanostructured electrocatalysts (Li et al., 2018) and bipolar membrane designs (Pătru et al., 2019) are strategies to achieve these goals. As the grid becomes more and more dependent on solar and wind energy, grid-connected electrolysers can also be a tool to buffer peaks and valleys in the energy supply. Although batteries and hydrogen electrolysers are a more obvious choice for this grid buffering application, CO₂ electrolysers have also been proposed (Centi et al., 2013; Lu and Jiao, 2016). CO₂ reduction products like formic acid are generally more energy-dense, safer and easier to store than hydrogen and, different from batteries, they can be used as seasonal buffers. CO₂ recovery and reuse in the reconversion of stored formic acid to electricity in a period of high electrical demand is essential to close the carbon cycle. Targets in formic acid electrolyser development for this grid buffering application include a high flexibility to accommodate a fluctuating power input. This is achieved by for example operating at ambient temperature and pressure and making the system modular. In another scenario, electrolysers can directly be coupled to a renewable power source such as solar PV panels ("PV-EC"). Energy losses by the Balance Of System are minimal and the current of the electrolyser can be matched to that of the solar PV cells, optimising in this way the solar-to-product efficiency like with solar hydrogen generators (Heremans et al., 2017). PV-EC devices are attractive for solar farms at remote locations. Formic acid is a candidate vector for transportation of the solar energy. Other candidates are hydrogen, ammonia, methane and methanol, each with their benefits and downsides (Thijs et al., 2021). Important benefits of formic acid are its transportability and high volumetric energy density compared to gaseous products. A complexity to consider is that CO₂ needs to be supplied to the remote location or generated *in situ* through for example direct air carbon capture (DACC). While DACC is interesting as a way to reduce the atmospheric CO₂ concentration, it requires a substantial amount of additional energy in the range of 1.4–2.8 kWh/kg CO₂ [International Energy Agency (IEA), 2021]. Combining

CO₂ capture and reduction into one device could reduce this energy demand, but this technology is still in an early phase (Kar et al., 2019; Sullivan et al., 2021). When developing PV-EC devices, the target is obtaining a high solar-to-product efficiency. This implies that the electrolyser should have a high energy efficiency and should operate close to the maximum power point of the PV cells it is connected to. Two approaches can be followed for achieving efficient connection. A large area of PV cells can be coupled to a small electrolyser such that it operates at a high current density. Highly active electrodes and low ohmic losses are needed for this approach and measures need to be taken to ensure that CO₂ is supplied to the active sites quickly. An alternative approach is to couple PV cells and an electrolyser of a similar size. Without solar concentration, PV cells deliver current densities in the range of a few mA/cm². At these low current densities, CO₂ supply to the cathode's active sites does not pose an issue and ohmic losses are low, which benefits the energy efficiency. Because the electrolyser is then large in size, its components such as the electrodes should be low cost. Important for this application is also the quality of the formic acid product. With different electrolysers, the product ranges from dilute aqueous potassium formate to high-concentration formic acid. To store and transport energy, the latter formulation is preferred. Formic acid and formate electrolyser concepts are shown in Figure 1. In a formate electrolyser (Figures 1A,B), CO₂ is converted at the cathode and a base, typically KOH, is converted at the anode. CO₂ and KOH are consumed to produce oxygen gas and potassium formate. There is a fundamental disadvantage to this, which is that downstream operations such as electro dialysis are needed to convert formate to formic acid and recover KOH. This complication lowers the overall process efficiency. Formic acid electrolysers (Figures 1C,D) directly produce formic acid from CO₂ and H₂O. Three compartment electrolysers (Figure 1D) are currently one of the most advanced designs, performing exceptionally well in terms of activity, selectivity and stability. In literature, three compartment electrolysers have been described with partial current densities up to 450 mA/cm² and stabilities of over 1,000 h, producing aqueous formic acid at a concentration exceeding 11 wt%. (Fan et al., 2020; Yang et al., 2020). They outperform designs like zero-gap electrolysers (Figure 1C) (Lee et al., 2015).

Here we report on a PV-EC device consisting of a three compartment electrolyser coupled with c-Si PV cells of similar-size. State-of-the-art three compartment electrolyser design is combined with a low cost anode and cathode electrode and commercially available solid electrolytes. The performance of the electrolyser is analysed in conditions relevant to direct PV coupling and current matching is done, maximising the solar-to-formic acid efficiency. Based on an analysis of the different components of the cell overpotential suggestions are made for further improvements.



2 Results and discussion

2.1 Cathode synthesis and H-cell characterisation

Electrochemical reduction of CO_2 to formate/formic acid is catalysed by metals like Sn, Bi, Pd, and Pb and their performance is enhanced through alloying, nanostructuring, exposing specific crystal facets and modifying the oxidation state. (Lu et al., 2014; Qiao et al., 2014; Du et al., 2017; Kumawat and Sarkar, 2017; Lee et al., 2020) Sn catalysts are known to combine a decent stability with a high selectivity in a broad range of electric potentials. Among the candidate metals, Sn is also one of the cheapest.

A Sn on Cu cathode was synthesised by electroplating Sn onto a porous Cu foam substrate. A copper support was selected for its high electric conductivity of 56 MS/m and convenience for use at large sizes. Cu foam is also flexible and not prone to crack, which is a common issue with e.g., carbon paper substrates. It has also been shown that a Sn film on Cu performs as well if not better as compared to pure Sn, which is attributed to Cu influencing the

surface oxidation state of Sn. (He et al., 2017; Morimoto et al., 2018) The constant current electrodeposition method used to deposit Sn onto Cu foam has been demonstrated by Wang et al. (2016) Characterisation with SEM-EDX reveals homogeneous, full coverage of the Cu foam with Sn particles ($<10 \mu\text{m}$) (Supplementary Figure S1). The electrode was evaluated in a three-electrode H-cell setup. The catholyte was 0.5 M KHCO_3 purged with CO_2 having a pH of 7.3. The selectivity of the electrochemical reduction reaction was determined with chronoamperometry at potentials in the range of -0.6 and -1.0 V versus RHE (Figure 2). In between each measurement, the catholyte was replaced with fresh CO_2 -saturated KHCO_3 . Product samples were taken after 30 min. The formate content was determined *via* ion chromatography. The overpotential for formate formation at a formate partial current density of 10 mA/cm^2 was ca. 0.52 V (-0.7 V vs. RHE). At an overpotential of 0.70 V (-0.9 V vs. RHE), the Sn/Cu electrode had a formate selectivity of over 65% and formate partial current density of ca. 70 mA/cm^2 . Hydrogen gas was the dominant by-product (Supplementary Figure S2). Note that the current density was

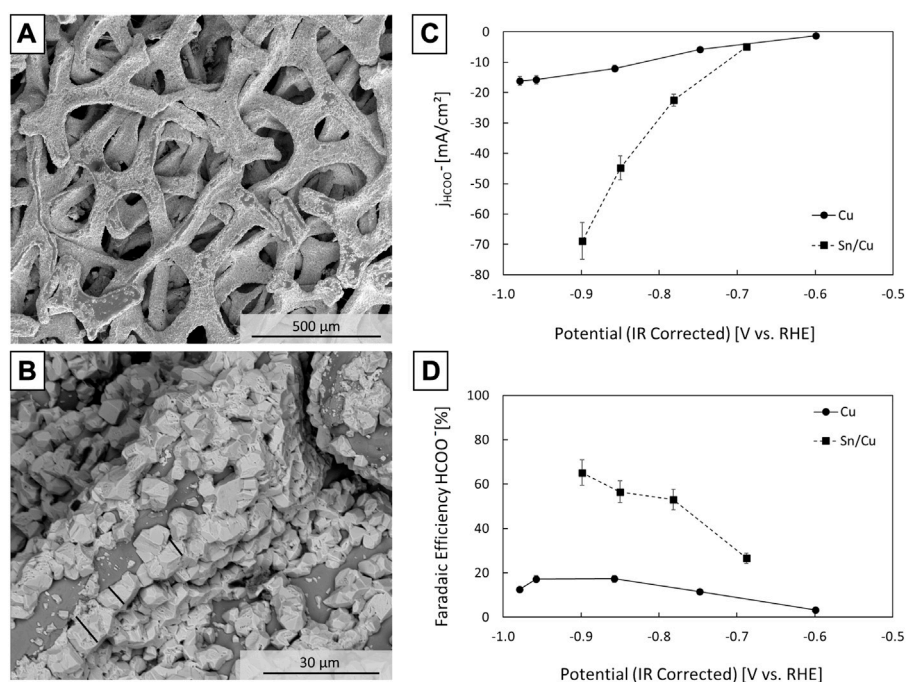


FIGURE 2

SEM images of the Sn/Cu cathode electrocatalyst (A,B), partial current densities (C) and formate faradaic efficiencies (D) against the IR corrected reduction potential in a H-cell setup with CO₂ saturated 0.5 M KHCO₃ catholyte. Formate was quantified via ion chromatography by sampling at the end of a 30 min measurement. The error bars correspond to the standard deviation on the ion chromatography measurements.

normalised to the geometric area of one side of the electrode, so this value for current density is high in comparison to literature sources that are often either normalised to the electrochemically active surface area or the real active surface area. (Zheng et al., 2020) The Cu foam itself had a faradaic efficiency for formate of below 17% in the potential range from -0.6 to -1.0 V vs. RHE (Figure 2), revealing that Sn added substantially to the selectivity. Comparison of the performance of our electrode with literature data (Supplementary Figure S3) revealed a moderate faradaic efficiency. For practical reasons we opted for a robust electrode to perform the demonstration. The cathode might be further improved by reducing the thickness of the Sn layer or by co-depositing Sn and Cu from a mixed CuCl₂-SnCl₂ solution. Zhao and Wang. (2016) observed a substantial influence of the thicknesses of the Sn film on Cu, and He et al. (2017) showed that a Cu_{0.2}Sn_{0.8} alloy performs better than pure Sn.

2.2 Anode synthesis and H-cell characterisation

At the anode, two types of electrocatalysts were used: an IrO₂/C nanoparticle catalyst and a NiFe catalyst. From the field of PEM electrolysis, it is known that IrO₂ is one of the few oxygen evolution reaction (OER) catalysts with high activity and stability

in acidic media. The IrO₂/C catalyst was synthesised by dropcasting an electrocatalyst ink containing IrO₂ nanoparticles, Nafion ionomer and isopropanol onto Toray carbon paper. The loading was ca. 2 mg IrO₂/cm². In a three-electrode setup with 0.5 M H₂SO₄ electrolyte saturated with O₂, IrO₂/C showed a high activity (Supplementary Figure S4). The overpotential for the OER was ca. 0.30 V at a current density of 10 mA/cm². This is comparable to literature, reporting overpotentials of IrO₂ nanoparticle catalysts at 10 mA/cm² of 0.29–0.33 V (Li et al., 2022). NiFe was used as an Earth-abundant alternative to IrO₂. The NiFe catalyst was synthesised by electroplating Ni and Fe from a Ni-Fe solution onto a porous Ni foam substrate, according to a procedure described in literature. (Solmaz and Kardaş, 2009; McCrory et al., 2015). In a three-electrode setup with 1 M KOH electrolyte saturated with O₂ the overpotential for the OER was ca. 0.27 V at a current density of 10 mA/cm² (Supplementary Figure S4). In liquid electrolyte, NiFe showed slightly higher activity than IrO₂/C.

Literature sources of three compartment electrolyzers use either an IrO₂ (Yang et al., 2017; Xia et al., 2019; Fan et al., 2020; Yang et al., 2020) or Pt (Yang et al., 2017; Fan et al., 2020) anode and oxidise either H₂SO₄, (Xia et al., 2019), H₂ (Fan et al., 2020) or H₂O. (Yang et al., 2017; Yang et al., 2020). To our knowledge, there are no earlier reports of three compartment electrolyzers where water is oxidised on an Earth abundant metal anode.

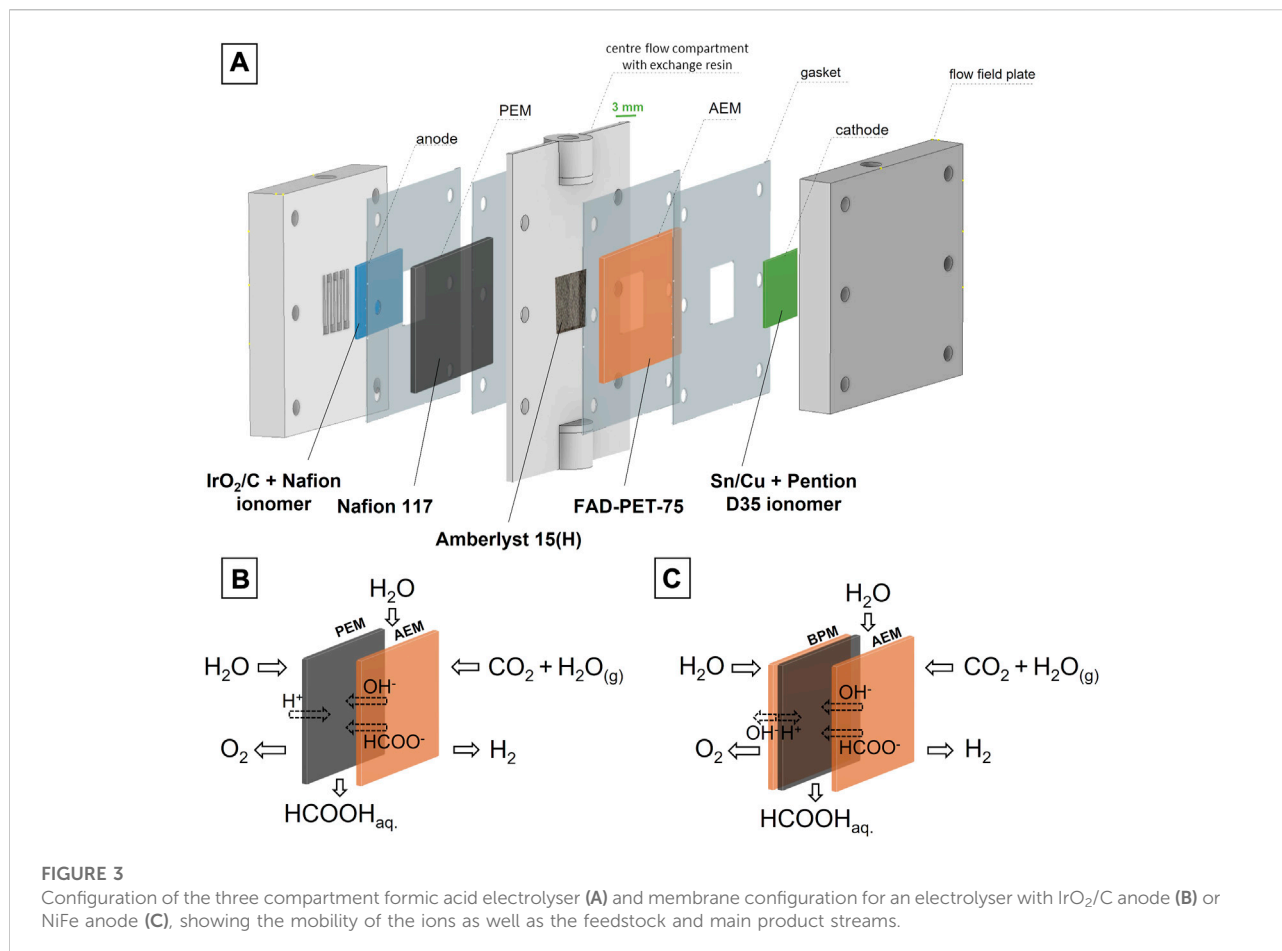


FIGURE 3

Configuration of the three compartment formic acid electrolyser (A) and membrane configuration for an electrolyser with IrO₂/C anode (B) or NiFe anode (C), showing the mobility of the ions as well as the feedstock and main product streams.

2.3 Electrolyser assembly and characterisation in conditions relevant to PV coupling

Three compartment electrochemical reactor cells were assembled using different materials. A scheme of a first setup with IrO₂/C anode and Sn/Cu cathode is shown in Figure 3. In between, there are three solid electrolytes: a Nafion 117 proton exchange membrane at the anode, a Fumasep FAD-PET-75 anion exchange membrane at the cathode and ion exchange resin beads (Amberlyst 15H) in between. Humidified CO₂ gas was conducted through the flow field of the cathode compartment. Liquid water was pumped through the anode and middle compartment. In a second setup with NiFe anode, the PEM was replaced with a bipolar membrane (BPM) combination of a Fumasep FAD-PET-75 membrane and Nafion 117 membrane (Figure 3). The anion exchange layer faced the anode, creating an alkaline environment in which the non-noble NiFe anode was stable.

The most innovative feature of a three compartment electrolyser is the use of ion exchange resin beads in the middle compartment. These beads are popular in

chromatography, water purification, waste water treatment and heterogeneous catalysis, but seldom used in electrolysers. Xia *et al.* (2019) reported the use of a non-specified porous styrene-divinylbenzene sulfonated copolymer (Fan *et al.*, 2020) and Kaczur *et al.* an amberlite IR-120 ion exchange resin. (Yang *et al.*, 2017; Yang *et al.*, 2020). A selection of candidate commercial ion exchanger beads were assessed for their conductivity. They were cation exchangers (Amberlyst 15H and Nafion NR-50H), anion exchangers (Amberlite IRA-402OH and IRN-78OH) and amphoteric (Dowex Retardion-11A8) ion exchangers. The conductivity *versus* the ion exchange capacity on a volumetric basis is displayed in Figure 4. As expected, the conductivity of the cation exchangers was significantly higher than that of the anion and amphoteric exchangers. Nafion NR-50H and Amberlyst 15H have nearly the same conductivity of ca. 23 mS/cm when saturated with liquid water. However, they have a very different bead size. Nafion NR-50H beads, with an average diameter of 3.7 mm when saturated with water (Supplementary Figure S5), were about ten times as large as Amberlyst-15H beads (ca. 300 μm). This has a strong influence on the contact area with the PEM and AEM. The smaller the beads, the more contact

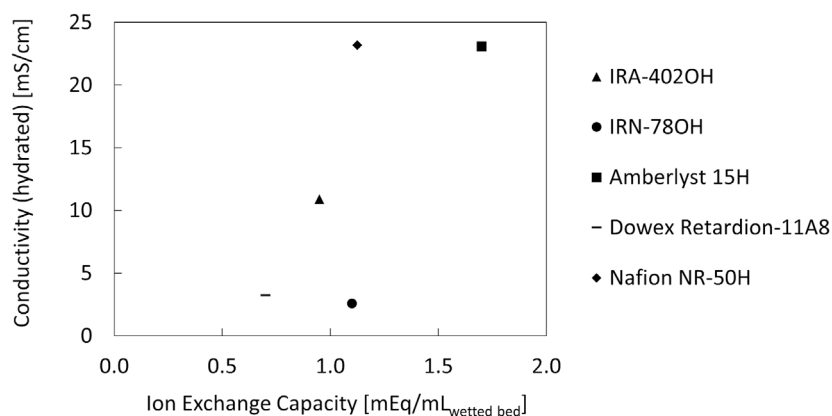


FIGURE 4 Conductivity of hydrated ion exchange resin beads, measured using electrochemical impedance spectroscopy.

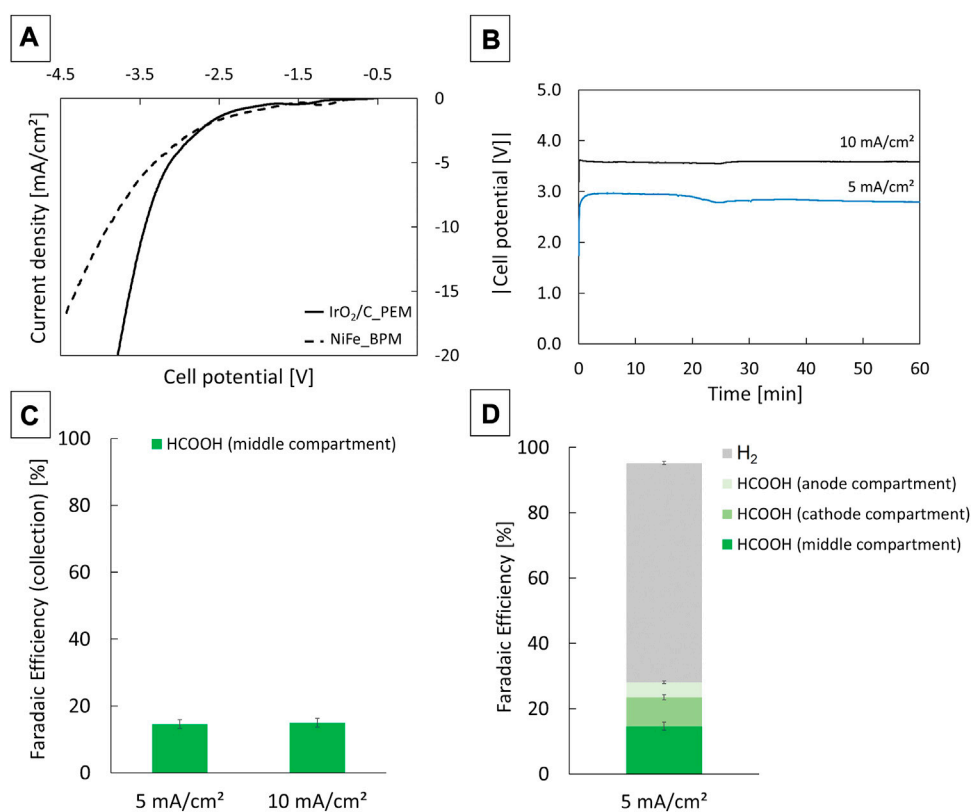


FIGURE 5 Polarization curves of a three compartment formic acid electrolyser with either IrO₂/C and a PEM or NiFe and a BPM at the anode side. Water was oxidised at the anode, humid CO₂ gas was reduced at the cathode. The scan rate was 5 mV/s (A). Cell potentials during chronopotentiometry measurements at 5 and 10 mA/cm² (B). Collection faradaic efficiency of formic acid from the middle compartment of the electrolyser (C) and total faradaic efficiency towards formic acid and hydrogen gas (D). Formic acid was quantified *via* ion chromatography by sampling at the end of a 60 min measurement, hydrogen was quantified *via* gas chromatography. The error bars correspond to the standard deviation on the ion- and gas chromatography measurements.

points between the beads and the membranes and among the beads themselves. This translates to a larger current density for smaller particles (Supplementary Figure S5). Reducing the bead size of Nafion NR-50H, for example by cryomilling, could improve its performance significantly. Here, we proceeded with Amberlyst 15H.

The activity of the three compartment formic acid electrolyser was investigated using cyclic voltammetry. The polarization curve of an electrolyser with an IrO₂/C anode and PEM are compared to that of an electrolyser with NiFe anode and BPM in Figure 5A. Owing to the presence of an additional anion exchange membrane layer in the latter case, the ionic resistance increased from 27.0 to 35.7 Ω·cm². From the IR corrected polarization curves (Supplementary Figure S6), it was also deduced that an additional anodic overpotential of ca. 0.38 V was required at 10 mA/cm². In liquid electrolytes where ionic contact is optimal, the activities of the NiFe anode and the IrO₂ anode were very similar. NiFe was even slightly more active (Supplementary Figure S4). This means that by improving the ionic contact between the NiFe anode and anion exchange membrane, the activity of the electrolyser with NiFe anode would be similar to that with an IrO₂ anode.

The formic acid selectivity was determined with chronopotentiometry in the low current density range (5 and 10 mA/cm²) relevant to direct PV coupling for an electrolyser with IrO₂/C anode (Figures 5B–D). It is assumed that changes in the anode materials have a limited effect on the product distribution on the cathode side of the reactor cell, so the selectivity measurements were not repeated for the NiFe anode. In the middle compartment of the reactor cell, the formation rate of formic acid amounted to about 14 and 28 μmol/cm²·h at 5 and 10 mA/cm², respectively. This corresponds to a collection faradaic efficiency of ca. 17% (Figure 5C). Some formic acid also crosses over through the PEM and AEM to the anode and cathode side, respectively. This was observed by analysing the water stream at the anode and leading the humid CO₂ stream at the cathode through a base trap. For the 5 mA/cm² case, of the total amount of formic acid only about half was collected in the water stream of the middle compartment. The anode and cathode stream contained formic acid corresponding to a faradaic efficiency of 4.6% and 8.9%, respectively (Figure 5D). Taking all formic acid streams into account, the faradaic efficiency was about 31% at 5 mA/cm². Most of the remaining current served hydrogen gas production (67%). Formic acid and hydrogen gas formation together account for about 98% of the total current (Figure 5D). A trace amount of methane was also detected but not quantified (Supplementary Figure S7). To sustain a current of 5 and 10 mA/cm², the cell potential was about 2.9 V and 3.6 V, respectively. The voltage remained more or less stable during the 60 min measurement time at the two current densities (Figure 5B).

2.4 Solar matching

The solar-to-product efficiency is the ratio between the energy that is stored in the product and the solar energy input. Here, we adopt two metrics for efficiency: solar-to-chemical efficiency (η_{STC}) and solar-to-formic acid efficiency (η_{STFA}). The STC efficiency is the percentage of solar energy that is stored in chemical bonds. It takes into account all chemical products. The remaining energy is dissipated as heat. The STFA efficiency is the percentage of solar energy that is stored in the chemical bonds of formic acid. These efficiencies are calculated as follows:

$$\eta_{\text{STC}} = \eta_{\text{coupling}} \cdot \eta_{\text{electrolysis}} \cdot \eta_{\text{PV}} = \frac{\sum_{i=0}^n (\Delta E_i^0 \cdot I_{\text{OP}} \cdot \text{FE}_i)}{P_{\text{sun}} \cdot A_{\text{PV}}}$$

$$\eta_{\text{STFA}} = \frac{\Delta E_{\text{HCOOH}}^0 \cdot I_{\text{OP}} \cdot \text{FE}_{\text{HCOOH}}}{P_{\text{sun}} \cdot A_{\text{PV}}}$$

In which FE_{*i*} is the faradaic efficiency for product *i*; ΔE_{*i*}⁰ the thermodynamic minimal cell voltage required to produce product *i*; I_{OP} the total operating current, P_{sun} the solar power density and A_{PV} the active area of the solar PV cells. ΔE⁰ for liquid formic acid and hydrogen gas is 1.48 V and 1.23 V respectively. He *et al.* pointed out that for comparing efficiencies of solar CO₂ electrolysers the current density should be normalised to the area of the PV cells. A small electrolyser powered with PV cells with a large area will have misleadingly large η_{STC} values when improperly normalised to the area of the electrolyser. (He and Janáky, 2020). Here, the area of the PV cells is considered for the solar energy input. η_{STC} and η_{STFA} are maximised by maximising the current at the operating point, I_{OP}. This is done by carefully matching the polarisation curve of the electrolyser with that of a series of solar cells. The operating point is the intersection point of the two curves. I_{OP} is maximised if the operating point is close to the maximum power point of the solar module. This matching is quantified by the coupling efficiency:

$$\eta_{\text{coupling}} = \frac{V_{\text{OP}} \cdot I_{\text{OP}}}{V_{\text{MPP}} \cdot I_{\text{MPP}}}$$

With MPP the maximum power point of the solar cell and OP the operating point.

This matching is illustrated in Figure 6. Commercial c-Si solar PV cells were used and calibrated close to 1 Sun intensity. For an individual cell, the open circuit voltage was about 0.65 V and the short circuit current 39 mA/cm² (Supplementary Figure S8). For an electrolyser with an IrO₂/C anode and PEM, the coupling efficiency was maximised at 95% with a series of 6 solar cells (Figure 6A). At the operating point, the cell voltage was 3.4 V and the photocurrent 38 mA. Normalised to the area of the solar PV cells, this equals a current density of 5.3 mA/cm². It equals 9.5 mA/cm² in the electrolysis unit. In this current range,

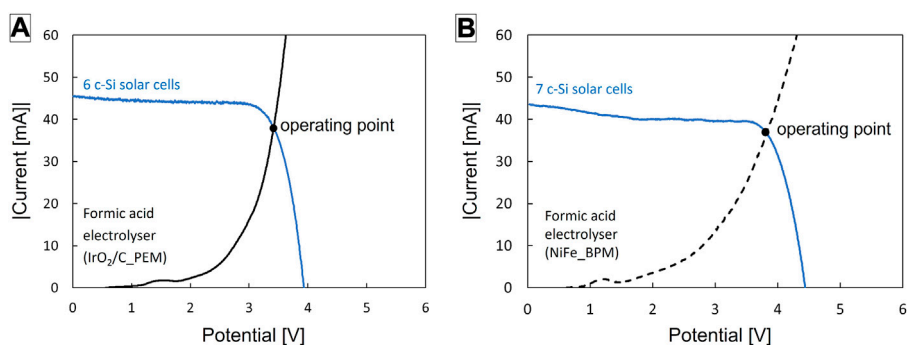


FIGURE 6

Matching of the polarisation curves of the electrolyzers with that of a series of solar cells to optimize the coupling efficiency and photocurrent, for the electrolyser with IrO₂/C anode and PEM (A) and the electrolyser with NiFe anode and BPM (B). The solar module was illuminated under 100 mW/cm² with a Xe lamp equipped with an infrared filter and air mass 1.5G filter. The solar cells had a surface area of 1.18 cm² each. The active geometric area of the electrodes was 4 cm².

TABLE 1 Literature on solar CO₂ electrolyzers producing formate, compared to this work on a solar CO₂ electrolyser producing dilute formic acid.

	This work	Ref. Kato et al. (2021)	Ref. Yang et al. (2018)	Ref. Piao et al. (2020)	Ref. Zhou et al. (2016)	Ref. Zhao et al. (2021)
	PV-EC	PV-EC	PV-EC	PV-EC	PEC	PV + PEC
PV cell type	c-Si	c-Si	GaInP/ GaInAs/Ge	c-Si		c-Si
Product [conc. (wt%)]	formic acid (0.02)	formate (-)	formate (0.01)	formate (0.07)	formate (-)	formate (-)
Anolyte	H ₂ O	0.4 M K-phosphate buffer	0.5 M NaHCO ₃	1 M KHCO ₃	1 M KOH	0.1 M KOH
Anode	NiFe	FTO/Ag/IrO _x	Ir/C	IrO ₂	GaAs/InGaP/TiO ₂ /Ni	single crystalline argon-treated TiO ₂
Polymer electrolyte membrane/assembly	Fumasep FAD-PET-75/Nafion 117/Amberlyst 15H IER/Fumasep FAD-PET-75	—	Selemon AEM	Nafion 117	Fumasep BPM	Nafion 117
Catholyte	H ₂ O vapour	0.4 M K-phosphate buffer	0.5 M NaHCO ₃	1 M KHCO ₃ + 0.1 M CsCl	2.8 M KHCO ₃	0.5 M KHCO ₃
Cathode	Sn/Cu	Ti/graphite/CS/MWCNTs/RuCP	Bi nanosheet	Bi dendrite	Ti mesh/C/Pd	BiOI-Bi
Current density [mA/cm ²]	4.4	6.4	1.9–3.0	12.0	8.5	1.1
Cell voltage [V]	3.8	1.9	2.5	2.7	2.0	(-)
Faradaic efficiency [%]	31 ^a	80 ^a	~100	>95%	94	97
Solar-to-product efficiency [%]	2.0	7.2	1.5	8.5	10.0	4.1

^aMajor by-product: H₂; (-): not specified.

we can assume that the electrolyser produces formic acid at ca. 31% faradaic efficiency and hydrogen gas at ca. 67% (Figure 5). Therefore, the STC efficiency was 7.0% and the STFA efficiency 2.4%. For an electrolyser with NiFe anode and BPM, the coupling

efficiency was maximised at 96% with a series of 7 solar cells (Figure 6B). At the operating point, the cell voltage was 3.8 V and the photocurrent 36 mA. Normalised to the area of the solar PV cells, this equals a current density of 4.4 mA/cm². Because of the

slightly lower photocurrent and use of a series of 7 solar cells, the STFA efficiency was slightly lower, *viz.* ca. 2.0%, and the STC efficiency 5.7%.

2.5 Literature comparison: solar efficiencies of CO₂ electrolyzers

Literature on solar CO₂ electrolyzers targeting CO formation is most abundant. Solar-to-CO efficiencies reach up to 19.1%. (Cheng et al., 2020) Solar CO₂ electrolyzers targeting formic acid are more scarce, with the large majority producing formate. A selection of what are, to our knowledge, the most efficient solar electrolyzers is given in Table 1. The highest reported solar-to-formate efficiency for a PV-EC electrolyser producing potassium formate is 7.2%. (Kato et al., 2021). Zhou et al. (2016) reported a remarkably high solar-to-formate efficiency of 10% with a PEC device. To our knowledge, this is the first work reporting on the efficiency of a solar CO₂ electrolyser without liquid salt solutions directly producing formic acid. Compared to other PV-EC devices the current density of our electrolyser is in the same order of magnitude, but the cell voltage is the highest by at least 1.3 V. The faradaic efficiency of 31% is rather low, with other CO₂ electrolyzers producing formate at faradaic efficiencies of over 80%. Owing to the near-optimal solar matching, the STFA efficiency of 2.0% is of average value. Like for other solar electrolyzers, the product concentration in this work is rather low (0.02 wt%). Formic acid of this concentration is only suited for a limited number of applications, such as feed for bioprocesses. (Thijs et al., 2022) The costs related to increasing the concentration by (extraction-) distillation processes are very high. (Ramdin et al., 2019; Thijs et al., 2022) Future research could focus on increasing the product concentration in the electrolyser stage by lowering the water flow rate in the middle compartment, which was not possible in the current experiments for technical reasons. In experiments in literature using similar three compartment lab scale electrolyzers, high formic acid concentrations in the percentage range have been reached (Fan et al., 2020).

2.6 Outlook on improvements

Several strategies can be followed to increase the STFA efficiency. With a faradaic efficiency for formic acid of 100%, the STFA efficiency of our electrolyser would be about 6.5%. Using more efficient multijunction PV cells would also lead to a substantial improvement. For hydrogen electrolyzers, solar-to-hydrogen efficiencies go up to 30% with solar

concentration and triple junction PV cells, which is about double compared to *c*-Si cells at 1 Sun, (Ager et al., 2015; Jia et al., 2016; Heremans et al., 2017; Khan et al., 2021b), although these cells are also significantly more expensive. Improvements can also be made by decreasing the cell potential required to drive the reaction, which would allow to use less *c*-Si cells in series, thereby increasing the efficiency. An experimental analysis was done to determine what components contribute most to the total cell potential.

When instead of H₂O and CO₂, 0.5 M H₂SO₄ and CO₂ saturated 0.5 M KHCO₃ solutions are fed to anode and cathode compartments respectively, the reaction conditions are similar to those in the H-cells in which the electrodes were individually characterised (subchapters 2.1 and 2.2). A polarization curve of such an electrolyser configuration is presented in Figure 7A. The ionic resistance measured with potentiostatic impedance spectroscopy was ca. 25.8 Ω.cm². At 10 mA/cm², this corresponds to an ohmic loss of 0.26 V. This shows that at least at low current densities, the ohmic losses in the three compartment solid electrolyte configuration are only a small contributor to the total cell potential. They could be even further reduced by decreasing the thickness of the middle compartment containing the ion exchanger beads, which was here 3 mm. Adding the standard reaction potential and the anode and cathode overpotential as determined in the H-cell setups, *viz.* 0.30 and 0.52 V, respectively, a total of 2.6 V is obtained. Experimentally, a comparable cell potential of about 2.7 V was required. When KHCO₃ at the cathode is replaced by CO₂ (Figure 7B), the cell potential increases to 3.7 V at 10 mA/cm², which is a significant increase by about 1 V. The ionic resistance increased only slightly (26.8 Ω.cm²). Replacing H₂SO₄ at the anode with H₂O (Figure 7B) does not further increase the cell potential. This implies that the large overpotential is a result of the cathode side operating in the absence of a liquid catholyte. Further research is needed to identify the exact cause of this. Possible explanations are an insufficient ionic contact between the cathode and the AEM, a lack of buffering capacity of the AEM as opposed to a bicarbonate solution leading to a high local pH, the absence of alkali cations to stabilize the CO₂ reduction intermediate or a lack of bicarbonate or water as a proton donor. Reducing this overpotential is key to significantly improve the STFA efficiency.

To circumvent this overpotential loss, the three compartment electrolyser could be operated with a catholyte solution, as shown in Figure 8. Because K⁺ cations are hindered from moving through the AEM, the catholyte will not readily be consumed. Rather, the (bi) carbonates will be constantly replenished by adding CO₂. At the low current densities of a PV-EC device as proposed in this work, the consumption rate of CO₂ is low. An air flow might contain enough CO₂ to maintain the catholyte at a

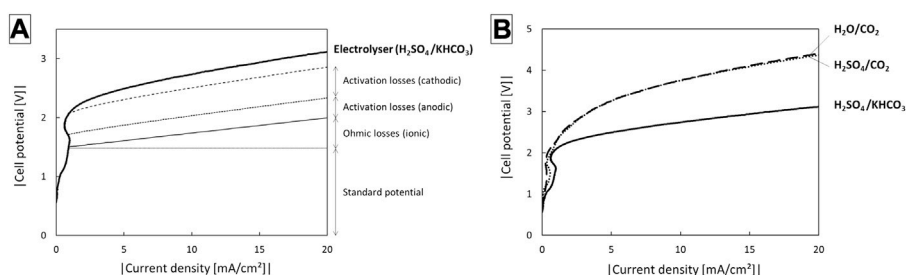


FIGURE 7

Electrolyser potential using different electrolyte compositions in the anode and cathode compartments of the three compartment electrolyser with IrO₂/C anode.

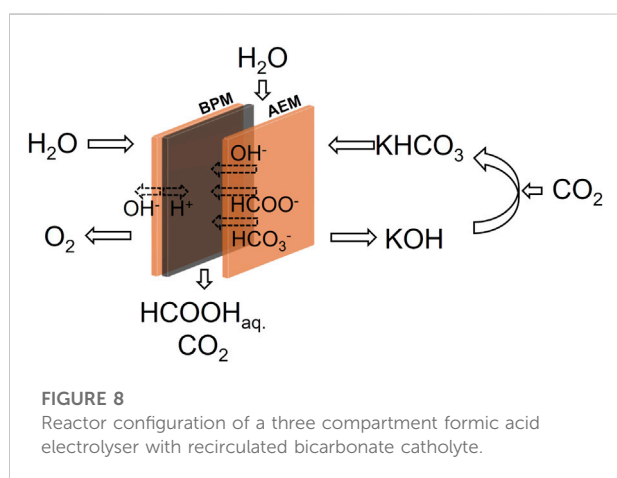


FIGURE 8

Reactor configuration of a three compartment formic acid electrolyser with recirculated bicarbonate catholyte.

stable (bi)carbonate concentration. This option needs further investigation. Additional research could focus on implementing a GDE-type electrode to improve the CO₂ availability or on implementing an AEM that absorbs as little K⁺ co-ions as possible (Geise et al., 2014).

3 Conclusion

In this work a first solar-driven electrolyser is demonstrated that directly produces formic acid from water and CO₂. The electrolyser consists of three compartments and uses only Earth abundant metals and commercially available solid electrolytes. It produces dilute formic acid at a solar-to-formic acid efficiency of 2%, with hydrogen gas as the major by-product. The overall solar-to-chemical efficiency is 5.7%. By producing formic acid instead of the common potassium formate, the need for downstream acidification steps is avoided. The dilute formic acid product is directly useable as feed for bioprocesses, or can be concentrated by an (extraction-) distillation process for use as a

liquid renewable fuel or chemical building block. By tuning the water flow in the middle compartment, the product concentration in the electrolyser stage could be increased to avoid the need for downstream processing completely.

An experimental analysis showed that a major part of the cell overpotential is due to the cathode compartment operating in the gas phase. Improving the cathode catalyst and its contact with the anion exchange membrane could result in a substantial improvement of the STEFA efficiency. Another perspective for improvement is the use of a catholyte. This could combine the benefits of a liquid phase reactor with the straight production of formic acid.

4 Materials and methods

4.1 Sn/Cu cathode

The Sn/Cu electrode was prepared by electroplating Sn from a SnCl₂-citrate solution onto a porous Cu foam substrate (MTI, 80 μm thickness, > 99.99% purity, 70%–80% porosity). The Cu foam was first cleaned by subsequent rinsing with ethanol, acetone and milli-Q water and drying in an oven at 60 °C for at least 1 h. Then, the foam was submerged in the electrolytic solution. The electrolytic solution was based on literature and was made by first dissolving sodium citrate dihydrate (≥99%) in milli-Q water (resistivity = 18.0 MΩ·cm) to a concentration of 0.05 M (Wang et al., 2016). Then the pH was adjusted to 6 by slowly adding droplets of a H₂SO₄ solution (50 vol%) while monitoring the pH. Finally, SnCl₂ (Honeywell, 98%) was added to a concentration of 0.018 M, after which the solution was stirred overnight. The electroplating of Sn was performed with a VersaSTAT 4 potentiostat (Princeton Applied Research) at a constant current of −4.8 mA/cm² for 35 min, with Cu foam as the working electrode and Pt as the counter electrode. Afterwards, the electrode was rinsed with milli-Q water.

The performance of the cathode was analysed in a H-cell setup. The H-cell operated at room temperature and was

connected to a potentiostat (Ametek VersaSTAT 3) with VersaStudio software. The anode and cathode compartment were filled with a 90 ml solution of 0.5 M H₂SO₄ and 0.5 M KHCO₃ (BioUltra, > 99.5%) respectively. The compartments were separated with a Nafion membrane (Nafion™ N117, Ion Power) that was prepared by boiling it in a 5% solution of H₂O₂, a 1 M H₂SO₄ solution and milli-Q water for one, two and 3 hours at 120°C respectively. The cathode compartment was pre-saturated with CO₂. During the experiments, it was continuously sparged with CO₂ at a flowrate of 20 ml/min, while under constant stirring. Graphite and Ag/AgCl (RE-1CP, saturated KCl, E_{Ag/AgCl} = 0.197 V) were used as the counter and reference electrode respectively. The reaction potential was converted to a reversible hydrogen electrode using the following formula:

$$\text{Potential (IR Corrected)} = E_{\text{vs. Ref.}} + E_{\text{Ref.}} + 0.059 \cdot \text{pH} - I_{\text{total}} \cdot R$$

The resistance R was measured with electrochemical impedance spectroscopy, which was performed at open circuit potential from 1 Mhz to 100 Hz. The resistance was found in the high frequency region where the imaginary impedance was 0.

4.2 IrO₂/C and NiFe anode

The IrO₂/C electrode for anodic water oxidation was made by synthesising an ink and dropcasting this onto a carbon paper support (Toray TP-060). The ink was synthesised by adding 100 mg of IrO₂ nanoparticles (FuelCellStore) to 960 µL of isopropanol (HPLC grade). 320 µL of a 5 wt% Nafion ionomer solution (FuelCellStore) was used as a binder. The ink was sonicated for 10 min. The carbon paper was rinsed with ethanol, acetone and milli-Q water and dried in an oven at 60°C for at least 1 h before dropcasting. 64 µL of ink was added per geometric cm² of carbon paper. The IrO₂ loading was determined by weighing before and after dropcasting. The NiFe electrode was prepared by electroplating Ni and Fe from a Ni-Fe solution onto a porous Ni foam substrate (PI-KEM, 1.6 mm thickness). The Ni foam was first cleaned by subsequent rinsing with ethanol, acetone and milli-Q water and drying in an oven at 60°C for at least 1 h. Then the foam was submerged in the electrolytic solution. The electrolytic solution was based on literature and consisted of NiSO₄·7 H₂O (120.6 g/L), NiCl₂·6 H₂O (3.3 g/L), H₃BO₃ (2.8 g/L), FeSO₄·7 H₂O (172.9 g/L) and FeCl₂·4 H₂O (3.6 g/L) in milli-Q water. (Solmaz and Kardaş, 2009). Then the pH was adjusted to 3 by slowly adding droplets of H₂SO₄ while monitoring the pH. The electrodeposition was performed under intensive stirring at a constant current of -50 mA/cm² for 680 s, with Ni foam as the working and counter electrode. Afterwards, the electrode was rinsed with milli-Q water.

The performance of the anodes was analysed in a H-cell setup. For IrO₂/C, the anode and cathode compartment were both filled with a 90 ml 0.5M H₂SO₄ solution. The compartments were separated with a Nafion 117 membrane. The anode compartment was pre-saturated with O₂. During the experiments, it was continuously sparged with O₂ at a flowrate of 20 ml/min, while under constant stirring. A Pt coil and Ag/AgCl (RE-1CP, saturated KCl, E_{Ag/AgCl} = 0.197 V) were used as the counter and reference electrode respectively. The performance of the NiFe anode was analysed in a 1M KOH solution sparged with O₂ and constantly stirred. A Pt coil and Hg/HgO (20 wt% NaOH, E-61AP, E_{Hg/HgO} = 0.124 V) electrode were used as the counter and reference electrode respectively.

4.3 Three compartment CO₂ electrolyser

4.3.1 Conductivity measurements of ion exchange resins

To determine the conductivity of the ion exchange resin beads, they were packed in a 7 mm thick layer in between two stainless steel plates. Cation and amphoteric exchangers (Amberlyst 15, Nafion NR-50 and Dowex Retardion-11A8) were hydrated with milli-Q water before the measurement. Anion exchangers (Amberlite IRA-402 and IRN-78) were ion-exchanged in a 1 M KOH electrolyte solution overnight and rinsed with milli-Q water. To ensure good contact between the beads and the plates, they were tightly pressed together and fastened with screws at an equal torque of 2 Nm. Potentiostatic EIS was used to determine the conductivity of the ion exchanger in between the plates. EIS was performed at open circuit potential from 1 Mhz to 100 Hz. The resistance was found in the high frequency region where the imaginary impedance was zero. The conductivity was calculated from resistance as follows:

$$\text{Conductivity} \left[\frac{\text{mS}}{\text{cm}} \right] = \frac{\text{thickness} [\text{cm}]}{R [\text{ohm}] \cdot \text{area} [\text{cm}^2]} \cdot 10^3$$

4.3.2 Reactor assembly

A commercially available reactor (FuelCellStore) was modified to contain three compartments. The reactor consisted of two graphite blocks with serpentine flow paths and gold-plated current collector plates on either side. A middle compartment was made in house by 3D printing. This compartment had a thickness of 3 mm with two slits (8 mm by 0.6 mm) to allow water to be pumped through. The reactor was assembled as shown in Figure 3. The geometric area of the electrodes was 4 cm². Milli-Q water was recirculated through the anode compartment with a peristaltic pump (Watson Marlow 205S) at a flowrate of 3.4 ml/min. A single-pass flow of milli-Q water was

pumped through the middle compartment at a flowrate of 0.2 ml/min with a syringe pump (WPI, Aladdin). Humid CO₂ gas flowed through the cathode compartment at 50 ml/min. The gas was humidified by flowing it through a glass humidifier at room temperature. To enhance the ionic contact between the cathode and the AEM, the cathode was coated with a layer of alkaline ionomer. The Sn/Cu electrode was dipped twice in a Pention D35 ionomer solution (FuelCellStore, 5 wt% in ethanol) with an intermediate drying step for several hours. Details on Pention D35 and SEM-imaging of the coated Sn/Cu electrode can be found in [Supplementary Figure S1](#). Before the reaction, the ionomer-coated cathode and AEM(s) were immersed in a 0.5 M KHCO₃ solution overnight to exchange the counterions to HCO₃⁻. Before use, they were thoroughly rinsed with milli-Q water. The Amberlyst 15H resin beads were hydrated with milli-Q water.

4.3.3 Product analysis

For gas quantification, the gases were brought from the reactor to a gas chromatograph (Interscience CompactGC 4.0). The chromatograph was equipped with a precolumn (Rt-QBond), molecular sieve column (Rt-Molsieve 5A) and thermal conductivity detector for analysis of permanent gases using argon carrier gas. The total flow was set at 5 ml/min. The volumetric concentrations of H₂ were determined from a linear calibration fitted over a range from 3 to 10 vol% H₂. The faradaic efficiency towards H₂ was calculated as follows:

$$FE(H_2) [\%] = \frac{P \cdot \frac{ml H_2}{RT} \cdot 10^{-6} \cdot 2 \cdot F}{I_{total}} \cdot 100$$

For formate/formic acid quantification, ion chromatography (Metrohm, Metrosep A Supp 4 anion separation column) was used. For liquid water streams, 1 M KOH was added dropwise until a pH > 6 was obtained to ensure that the product, with a pKa of 3.75, was completely dissociated for analysis through ion chromatography. Gas flows were connected to a base trap filled with 10 ml of a 0.1 M KHCO₃ solution (pH ~ 6.8), from which was sampled after the reaction for analysis. The faradaic efficiency towards formate (at moment t) was calculated as follows:

$$FE_{HCOO^-} [\%] = \frac{mol HCOO_t^- \cdot 2 \cdot F}{charge\ passed_t [C]} \cdot 100$$

(Partial) current densities were normalised to the geometric surface area of one side of the electrode, unless stated otherwise:

$$j_{HCOO^-} = \frac{I_{total} \cdot \frac{FE_{HCOO^-}}{100}}{electrode\ surface\ area_{geom.;\ 1\ side}}$$

Data availability statement

The raw data supporting the conclusion of this article will be made available by the authors, without undue reservation.

Author contributions

JM and JR initiated and supervised the research and contributed to the writing. BT performed the experiments and contributed to the writing. LH, GH, and WW contributed to the experiments and approved the manuscript for publication.

Funding

This research was funded by CO2PERATE, a cluster SBO project (No. HBC. 2017.0692) supported by Vlaams Agentschap Innoveren en Ondernemen (VLAIO).

Acknowledgments

JM acknowledges the Flemish government for long term structural funding (Methusalem program).

Conflict of interest

The authors declare that the research was conducted in the absence of any commercial or financial relationships that could be construed as a potential conflict of interest.

Publisher's note

All claims expressed in this article are solely those of the authors and do not necessarily represent those of their affiliated organizations, or those of the publisher, the editors and the reviewers. Any product that may be evaluated in this article, or claim that may be made by its manufacturer, is not guaranteed or endorsed by the publisher.

Supplementary material

The Supplementary Material for this article can be found online at: <https://www.frontiersin.org/articles/10.3389/fceng.2022.1028811/full#supplementary-material>

References

- Ager, J. W., Shaner, M. R., Walczak, K. A., Sharp, I. D., and Ardo, S. (2015). Experimental demonstrations of spontaneous, solar-driven photoelectrochemical water splitting. *Energy Environ. Sci.* 8 (10), 2811–2824. doi:10.1039/c5ee00457h
- Centi, G., Quadrelli, E. A., and Perathoner, S. (2013). Catalysis for CO₂ conversion: A key technology for rapid introduction of renewable energy in the value chain of chemical industries. *Energy Environ. Sci.* 6 (6), 1711–1731. doi:10.1039/c3ee00056g
- Cheng, W., Richter, M. H., Sullivan, I., Larson, D. M., Xiang, C., Brunschwig, B. S., et al. (2020). CO₂ reduction to CO with 19% Efficiency in a solar-driven gas diffusion electrode flow cell under outdoor solar illumination. *ACS Energy Lett.* 5 (5), 470–476. doi:10.1021/acsenerylett.9b02576
- Du, D., Lan, R., Humphreys, J., and Tao, S. (2017). Progress in inorganic cathode catalysts for electrochemical conversion of carbon dioxide into formate or formic acid. *J. Appl. Electrochem.* 47 (6), 661–678. doi:10.1007/s10800-017-1078-x
- Fan, L., Xia, C., Zhu, P., Lu, Y., and Wang, H. (2020). Electrochemical CO₂ reduction to high-concentration pure formic acid solutions in an all-solid-state reactor. *Nat. Commun.* 11 (1), 3633–3639. doi:10.1038/s41467-020-17403-1
- García de Arquer, F. P., Dinh, C.-T., Ozden, A., Wicks, J., McCallum, C., Kirmani, A. R., et al. (2020). CO₂ electrolysis to multicarbon products at activities greater than 1 A cm⁻². *Science* 367 (6478), 661–666. doi:10.1126/science.aay4217
- Geise, G. M., Cassidy, H. J., Paul, D. R., Logan, B. E., and Hickner, M. A. (2014). Specific ion effects on membrane potential and the permselectivity of ion exchange membranes. *Phys. Chem. Chem. Phys.* 16 (39), 21673–21681. doi:10.1039/c4cp03076a
- Global Formic Acid Market Report (2022). Formic acid market by product types (grades of 85%, 94%, 99%, and others), applications (agriculture, leather & textile, rubber, chemical & pharmaceuticals, and others), and regions (Asia Pacific, North America, Latin America, Europe, and Middle East & Africa) – global industry analysis, growth, share, size, trends, and forecast, 2021–2028. Available from: <https://www.industryresearch.biz/global-formic-acid-market-18873267>.
- He, J., Dettelbach, K. E., Huang, A., and Berlinguette, C. P. (2017). Brass and bronze as effective CO₂ reduction electrocatalysts. *Angew. Chem. Int. Ed. Engl.* 56 (52), 16806–16809. doi:10.1002/ange.201709932
- He, J., and Janáky, C. (2020). Recent advances in solar-driven carbon dioxide conversion: Expectations versus reality. *ACS Energy Lett.* 5 (6), 1996–2014. doi:10.1021/acsenerylett.0c00645
- Heremans, G., Trompoukis, C., Daems, N., Vankelecom, I. F. J., Martens, A., Rong, J., et al. (2017). Vapor-fed solar hydrogen production exceeding 15% efficiency using Earth abundant catalysts and anion exchange membrane. *Sustain. Energy Fuels* 1, 2061–2065. doi:10.1039/c7se00373k
- Higgins, D., Hahn, C., Xiang, C., Jaramillo, T. F., and Weber, A. Z. (2019). Gas-diffusion electrodes for carbon dioxide reduction: A new paradigm. *ACS Energy Lett.* 4 (1), 317–324. doi:10.1021/acsenerylett.8b02035
- International Energy Agency (IEA) (2021). Direct air capture. Available from: <https://www.iea.org/reports/direct-air-capture>.
- Jia, J., Seitz, L. C., Benck, J. D., Huo, Y., Chen, Y., Ng, J. W. D., et al. (2016). Solar water splitting by photovoltaic-electrolysis with a solar-to-hydrogen efficiency over 30%. *Nat. Commun.* 7, 13237. doi:10.1038/ncomms13237
- Kar, S., Goepfert, A., and Prakash, G. K. S. (2019). Integrated CO₂ capture and conversion to formate and methanol: Connecting two threads. *Acc. Chem. Res.* 52 (10), 2892–2903. doi:10.1021/acs.accounts.9b00324
- Kato, N., Mizuno, S., Shiozawa, M., Nojiri, N., Kawai, Y., Fukumoto, K., et al. (2021). A large-sized cell for solar-driven CO₂ conversion with a solar-to-formate conversion efficiency of 7.2%. *Joule* 5 (3), 687–705. doi:10.1016/j.joule.2021.01.002
- Khan, M. A., Al-Shankiti, I., Ziani, A., and Idriss, H. (2021). Demonstration of green hydrogen production using solar energy at 28% efficiency and evaluation of its economic viability. *Sustain. Energy Fuels* 5 (4), 1085–1094. doi:10.1039/d0se01761b
- Khan, S., Hwang, J., Horn, Y., and Kripa, K. (2021). Catalyst-proximal plastrons enhance activity and selectivity of carbon dioxide electroreduction. *Cell. Rep. Phys. Sci.* 2 (2), 100318. doi:10.1016/j.xcrp.2020.100318
- Kumawat, A. S., and Sarkar, A. (2017). Comparative study of carbon supported Pb, Bi and Sn catalysts for electroreduction of carbon dioxide in alkaline medium. *J. Electrochem. Soc.* 164 (14), H1112–H1120. doi:10.1149/2.0991714jes
- Lee, M. Y., Park, K. T., Lee, W., Lim, H., Kwon, Y., and Kang, S. (2020). Current achievements and the future direction of electrochemical CO₂ reduction: A short review. *Crit. Rev. Environ. Sci. Technol.* 50 (8), 769–815. doi:10.1080/10643389.2019.1631991
- Lee, S., Ju, H. K., Machunda, R., Uhm, S., Lee, J. K., Lee, H. J., et al. (2015). Sustainable production of formic acid by electrolytic reduction of gaseous carbon dioxide. *J. Mat. Chem. A Mat.* 3 (6), 3029–3034. doi:10.1039/c4ta03893b
- Li, A., Kong, S., Guo, C., Ooka, H., Adachi, K., Hashizume, D., et al. (2022). Enhancing the stability of cobalt spinel oxide towards sustainable oxygen evolution in acid. *Nat. Catal.* 5, 109–118. doi:10.1038/s41929-021-00732-9
- Li, F., MacFarlane, D. R., and Zhang, J. (2018). Recent advances in the nanoengineering of electrocatalysts for CO₂ reduction. *Nanoscale* 10 (14), 6235–6260. doi:10.1039/c7nr09620h
- Lu, Q., and Jiao, F. (2016). Electrochemical CO₂ reduction: Electrocatalyst, reaction mechanism, and process engineering. *Nano Energy* 29, 439–456. doi:10.1016/j.nanoen.2016.04.009
- Lu, X., Leung, D. Y. C., Wang, H., Leung, M. K. H., and Xuan, J. (2014). Electrochemical reduction of carbon dioxide to formic acid. *ChemElectroChem* 1 (5), 836–849. doi:10.1002/celc.201300206
- McCrorry, C. C. L., Jung, S., Ferrer, I. M., Chatman, S. M., Peters, J. C., and Jaramillo, T. F. (2015). Benchmarking hydrogen evolving reaction and oxygen evolving reaction electrocatalysts for solar water splitting devices. *J. Am. Chem. Soc.* 137 (13), 4347–4357. doi:10.1021/ja510442p
- Morimoto, M., Takatsuji, Y., Yamasaki, R., Hashimoto, H., Nakata, I., Sakakura, T., et al. (2018). Electrodeposited Cu-Sn alloy for electrochemical CO₂ reduction to CO/HCOO. *Electrocatalysis* 9, 323–332. doi:10.1007/s12678-017-0434-2
- Pátru, A., Binninger, T., Pribyl, B., and Schmidt, T. J. (2019). Design principles of bipolar electrochemical Co-electrolysis cells for efficient reduction of carbon dioxide from gas phase at low temperature. *J. Electrochem. Soc.* 166 (2), F34–F43. doi:10.1149/2.1221816jes
- Piao, G., Yoon, S. H., Han, D. S., and Park, H. (2020). Ion-enhanced conversion of CO₂ into formate on porous dendritic bismuth electrodes with high efficiency and durability. *ChemSusChem* 13, 698–706. doi:10.1002/cssc.201902581
- Qiao, J., Liu, Y., Hong, F., and Zhang, J. (2014). A review of catalysts for the electroreduction of carbon dioxide to produce low-carbon fuels. *Chem. Soc. Rev.* 43 (2), 631–675. doi:10.1039/c3cs60323g
- Ramdin, M., Morrison, A. R. T., De Groen, M., Van Haperen, R., De Kler, R., Irtem, E., et al. (2019). High-pressure electrochemical reduction of CO₂ to formic acid/formate: Effect of pH on the downstream separation process and economics. *Ind. Eng. Chem. Res.* 58 (51), 22718–22740. doi:10.1021/acs.iecr.9b03970
- Solmaz, R., and Kardaş, G. (2009). Electrochemical deposition and characterization of NiFe coatings as electrocatalytic materials for alkaline water electrolysis. *Electrochim. Acta* 54 (14), 3726–3734. doi:10.1016/j.electacta.2009.01.064
- Song, J. T., Song, H., Kim, B., and Oh, J. (2019). Towards higher rate electrochemical CO₂ conversion: From liquid-phase to gas-phase systems. *Catalysts* 9 (9), 224. doi:10.3390/catal9030224
- Sullivan, I., Goryachev, A., Digdaya, I. A., Li, X., Atwater, H. A., Vermaas, D. A., et al. (2021). Coupling electrochemical CO₂ conversion with CO₂ capture. *Nat. Catal.* 4, 952–958. doi:10.1038/s41929-021-00699-7
- Thijs, B., Houllberghs, M., Hollevoet, L., Heremans, G., Rongé, J., and Martens, J. A. (2021). 2 hydrogen, fueling the future: Introduction to hydrogen production and storage techniques. *Hydrogen Storage Sustain.* 2, 159–194. doi:10.1515/9783110596281-010
- Thijs, B., Rongé, J., and Martens, J. (2022). Matching emerging formic acid synthesis processes with application requirements. *Green Chem.* 24 (24), 2287–2295. doi:10.1039/d1gc04791d
- Wang, Y., Zhou, J., Lv, W., Fang, H., and Wang, W. (2016). Electrochemical reduction of CO₂ to formate catalyzed by electroplated tin coating on copper foam. *Appl. Surf. Sci.* 362, 394–398. doi:10.1016/j.apsusc.2015.11.255
- Xia, C., Zhu, P., Jiang, Q., Pan, Y., Liang, W., Stavitsk, E., et al. (2019). Continuous production of pure liquid fuel solutions via electrocatalytic CO₂ reduction using solid-electrolyte devices. *Nat. Energy* 4 (9), 776–785. doi:10.1038/s41560-019-0451-x
- Yang, H., Han, N., Deng, J., Wu, J., Wang, Y., Hu, Y., et al. (2018). Selective CO₂ reduction on 2D mesoporous Bi nanosheets. *Adv. Energy Mat.* 8 (35), 1801536–6. doi:10.1002/aenm.201801536

Yang, H., Kaczur, J. J., Sajjad, S. D., and Masel, R. I. (2017). Electrochemical conversion of CO₂ to formic acid utilizing Sustainion™ membranes. *J. CO₂ Util.* 20, 208–217. doi:10.1016/j.jcou.2017.04.011

Yang, H., Kaczur, J. J., Sajjad, S. D., and Masel, R. I. (2020). Performance and long-term stability of CO₂ conversion to formic acid using a three-compartment electrolyzer design. *J. CO₂ Util.* 42, 101349. doi:10.1016/j.jcou.2020.101349

Yue, P., Fu, Q., Li, J., Zhang, L., Xing, L., Kang, Z., et al. (2021). Triple-phase electrocatalysis for the enhanced CO₂ reduction to HCOOH on a hydrophobic surface. *Chem. Eng. J.* 405, 126975. doi:10.1016/j.cej.2020.126975

Zhao, C., and Wang, J. (2016). Electrochemical reduction of CO₂ to formate in aqueous solution using electro-deposited Sn catalysts. *Chem. Eng. J.* 293, 161–170. doi:10.1016/j.cej.2016.02.084

Zhao, J., Xue, L., Niu, Z., Huang, L., Hou, Y., Zhang, Z., et al. (2021). Conversion of CO₂ to formic acid by integrated all-solar-driven artificial photosynthetic system. *J. Power Sources* 512, 230532. doi:10.1016/j.jpowsour.2021.230532

Zheng, W., Liu, M., and Lee, L. Y. S. (2020). Best practices in using foam-type electrodes for electrocatalytic performance benchmark. *ACS Energy Lett.* 5 (10), 3260–3264. doi:10.1021/acsenergylett.0c01958

Zhou, X., Liu, R., Sun, K., Chen, Y., Verlage, E., Francis, S. A., et al. (2016). Solar-driven reduction of 1 atm of CO₂ to formate at 10% energy-conversion efficiency by use of a TiO₂-protected III-V tandem photoanode in conjunction with a bipolar membrane and a Pd/C cathode. *ACS Energy Lett.* 1 (4), 764–770. doi:10.1021/acsenergylett.6b00317